# Understanding the Chemo-Mechanical Function of Silver-Carbon Interlayer in Sheet-type All-Solid-State Lithium-Metal Batteries

*Chaoshan Wu,[†,1] Benjamin Emley,[†,1] Lihong Zhao,[1,2] Yanliang Liang,[1,2] Qing Ai,[3] Zhaoyang Chen,[1] Francisco C Robles Hernández,[4] Fei Wang,[1] Samprash Risal,[1] Hua Guo,[3] Jun Lou,[3] Yan Yao, [1,2]* Zheng Fan[4,]**

[1] Materials Science and Engineering Program and Texas Center for Superconductivity at the University of Houston, University of Houston, 4726 Calhoun Rd, Houston, Texas 77204, USA

[2] Department of Electrical and Computer Engineering, University of Houston, 4726 Calhoun Rd, Houston, Texas 77204, USA

[3] Department of Materials Science and Nano Engineering, Rice University, 6100 Main St MS 364, Houston, TX 77005, USA

[4] Department of Engineering Technology, University of Houston, Houston, TX 77204, USA

[†] C.W. and B.E. contributed equally.

* Corresponding author: yyao4@uh.edu, fanzheng@uh.edu

**ABSTRACT**

All-solid-state batteries with lithium metal anodes hold great potential for high-energy battery applications. However, forming and maintaining stable solid-solid contact between lithium anode and solid electrolyte remains a major challenge. One promising solution is the use of a silver-carbon (Ag-C) interlayer, but its chemo-mechanical properties and impact on interface stabilities need to be comprehensively explored. Here, we examine the function of Ag-C interlayers in addressing interfacial challenges using various cell configurations. Experiments show that the interlayer improves interfacial mechanical contact, leading to a uniform current distribution and suppressing lithium dendrites growth. Furthermore, the interlayer regulates lithium deposition in the presence of Ag particles via improved Li diffusivity. The sheet-type cells with the interlayer achieve a high energy density of 514.3 Wh $L^{-1}$ and an average Coulombic efficiency of 99.97% over 500 cycles. This work provides insights into the benefits of using Ag-C interlayers for enhancing the performance of all-solid-state batteries.

**KEYWORDS**

All-solid-state lithium metal batteries; interlayer; silver-carbon composite; sheet-type solid-state cells

All-solid-state lithium metal batteries hold great promise for electric vehicles (EVs) with long-range capability and improved safety.[1,2] Solid-state electrolytes play an important role in all-solid-state batteries. The solid-state battery design significantly increases the energy density when combined with lithium metal anode with an extremely high capacity (3860 mAh $g^{-1}$) and lowest redox potential (-3.04 V *vs.* standard hydrogen potential).[3,4] Among a plethora of promising solid-state electrolytes, sulfide-based solid electrolytes stand out for their remarkable ionic conductivity, low cost, and exceptional processability.[5] The argyrodite-type sulfide electrolytes, such as $Li_6PS_5Cl$ (LPSCl), have comparable room-temperature Li-ion conductivities (3 mS $cm^{-1}$) to those of non-aqueous liquid electrolytes.[6] Despite its high ionic conductivity, realizing high-performance all-solid-state lithium metal batteries with sulfide electrolytes remains difficult due to the poor solid-solid contact between the Li anode and solid electrolytes. The contact problem is caused by the inherent surface roughness of lithium metal and electrolyte, which increases interfacial impedance and acts as a precursor for lithium dendritic growth.[7] The formation of voids during lithium stripping on the Li anode deteriorates the metal–electrolyte contact even further.[8]

To date, numerous investigations of metal–electrolyte contact in all-solid-state batteries have focused on the development of interfacial engineering strategies. Between the Li anode and solid electrolyte, a mixed ionic-electronic conductor (MIEC) interlayer has been introduced to buffer mechanical strain, promote interfacial contact, alleviate chemical instability, improve stripping/plating homogeneity, and therefore suppress lithium dendrite formation and propagation.[9-12] Lee *et al.* first reported the screen-printed silver-carbon (Ag-C) composite as an interlayer between the anode current collector and the electrolyte, allowing a high current density (3.4 mA/$cm^2$) over 1000 cycles with a consistent Coulombic efficiency greater than 99.8%.[9] Li *et al.* pointed out that Ag-C composite possesses an MIEC scaffold nature that regulates Li

transport.[10, 13] In addition, efforts were made to comprehend the contributions of carbon black (CB), metal particles, and binders to the Ag-C interlayer. The choice of metal was found to affect lithium growth location and the binding force between the interlayer and electrolyte determines structural integrity during lithium plating [11,12] Suzuki *et al*. studied various metal-added carbon composite anodes for solid-state cells and concluded that Ag outperforms other metals (*e.g.*, Zn, Sn, Al, Ni) in suppressing short circuits.[11] Oh *et al*. identified the binder effects in Ag-C composite that allow a strong binding force and an effective buffering of the volume change in the electrode, thus preventing the formation of cracks and enabling the battery with improved mechanical stability and long-term cyclability.[12] Despite the growing interest in exploring the Ag-C interlayer, knowledge of its stable interface mechanisms remains insufficient. This understanding is key to scalable, high-performance solid-state lithium metal batteries.

In this study, we report for the use of spray coated Ag-C interlayers for sheet-type all-solid-state lithium metal cells, as well as an investigation of the chemo-mechanical role of the Ag-C interlayer in addressing Li-electrolyte interfacial challenges. The Ag-C interlayer improves the interfacial contact between Li anode and solid electrolyte, thereby homogenizing the $Li^+$ flux and suppressing the lithium dendrite growth. This was confirmed by running controlled experiments on a variety of testing cell configurations to examine the Li-electrolyte interface evolutions under the conditions with and without the interlayer. Furthermore, controlled studies between pure carbon interlayer and Ag-C interlayer show that the presence of Ag metal improves Li diffusivity, indicating that Ag metal plays a critical role in regulating lithium deposition in solid-state cells. These discoveries lead to the rational design of Ag-C interlayers, which significantly improve the electrochemical performance of sheet-type solid-state cells, presenting a promising strategy for the scalable production of high-energy solid-state batteries.

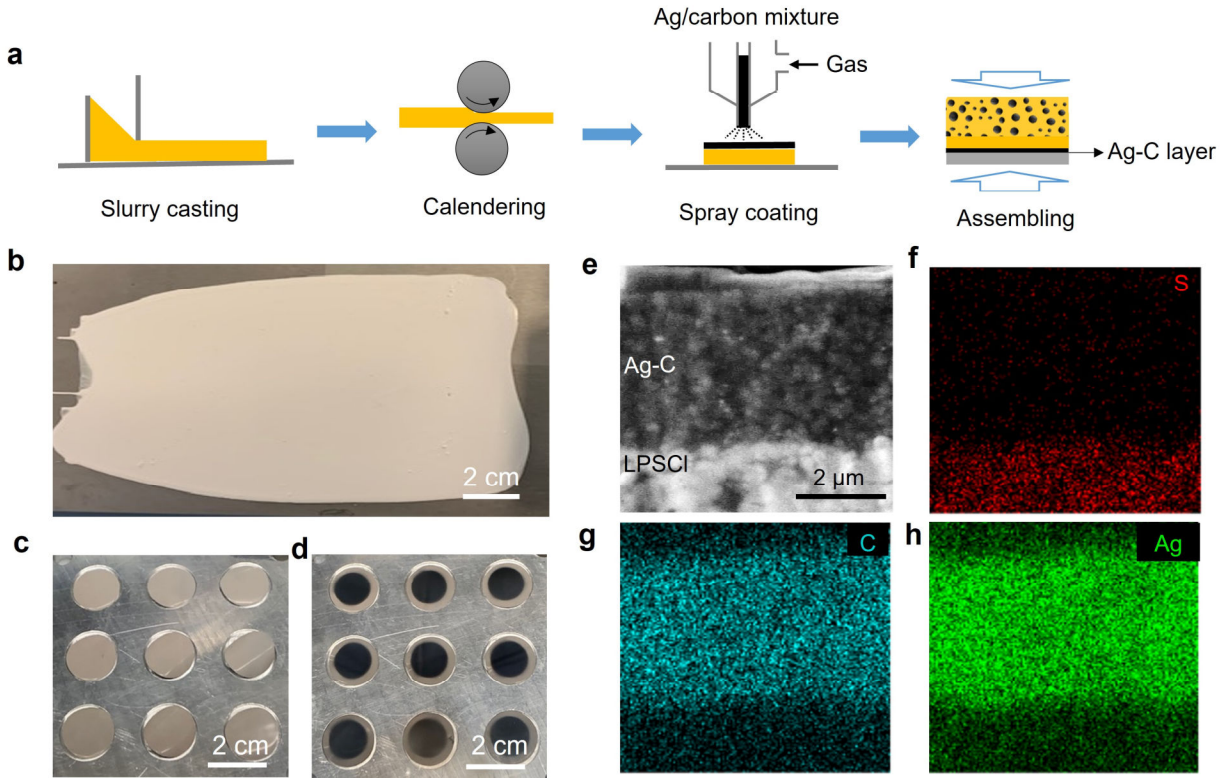


**Figure 1**. **Fabrication and characterization of Ag-C | LPSCl bilayer composites.** (a) The fabrication steps involve slurry casting, calendaring, spray coating of an Ag-carbon layer, drying, and final assembling. (b-c) Optical images of free-standing LPSCl thin films. (d) Nine samples of the Ag-C | LPSCl bilayer composite. (e) Cross-sectional SEM and (f-h) EDS mapping of the Ag-C|LPSCl bilayer composites.

## Fabrication of Ag-C | LPSCl bilayer composites

LPSCl electrolyte attracts much attention due to its superior ionic conductivity and self-passivation interface with the Li anode. In this work, we used a slurry-based method to create sheet-type solid electrolyte film (**Figure 1a**).[14] Briefly, a solid electrolyte sheet was fabricated by tape-casting electrolyte slurries onto a silicone-coated poly(ethylene terephthalate) (PET) substrate. LPSCl powders, hydrogenated nitrile butadiene rubber (HNBR), and a 50:50 w/w mixture of anhydrous toluene and isobutyl isobutyrate are mixed to form the slurry. The solid electrolyte sheets were calendared and cut into desired sizes with a hollow punch after drying in vacuum (**Figures 1b** and **1c**). The solid electrolyte sheet was calendared and densified at 375 MPa.

We observed a typical thickness reduction of  50%, resulting in a thickness of 40 μm after calendaring.

The Ag-C slurry was then spray coated onto one side of the solid electrolyte sheet via an air-brush technique with Argon carrier gas. The Ag-C slurry was prepared by mixing nano-silver particles (60 nm in diameter), carbon black particles, and HNBR in a 5 wt. % ratio with the same solvent mixture used for solid electrolyte coating. The total solid content of the slurry was 12 wt. %. The Ag-C coated solid electrolyte sheets were removed from the PET substrate and vacuum dried (**Figure 1d**). We developed an air-free vessel to transport samples from the glovebox and a Helios SEM/FIB. The bilayer films were examined with a cross-sectional SEM (**Figure 1e**). The Ag-C layer has a thickness of about 5 μm. The element distribution of silver, carbon, and sulfur is shown by EDS mapping. We used spray coating as a scalable technique that eliminates the need for free-standing films and lamination. This method has the potential to tackle some of the challenges associated with large-scale production of SSBs, particularly scalability and uniformity.[15,16] In comparison to screen printing,[9] the spray coating method demonstrated in this study offers superior uniformity and greater flexibility in controlling the interlayer thickness.[17] Furthermore, with spray coating, waste is significantly reduced, and the starting material is efficiently utilized in fabricating of the active film.[18]

**Improving mechanical contact with the interlayer**

During solid-state cell fabrication, interfacing lithium metal with solid electrolyte to form an intimate contact remains a significant challenge. According to Meng *et al*., stacking pressure is critical in forming excellent contact between the lithium anode and solid electrolyte.[19] The optimum stacking pressure introduces better contact. Inadequate contact may cause high local current density during charge and discharge, resulting in void formation and dendrite growth. The

optimum pressure is highly dependent on the electrolyte thickness because a thinner pellet is more susceptible to short circuits due to the significantly shorter path of length for the extruded lithium, even at lower stack pressures. It is very likely that Li will infiltrate the thin electrolyte during cell fabrication before intimate contact between the metal and electrolyte can be established (**Figure S1**).[20] Under low stack pressure, we hypothesize that the excellent deformability of Ag-C interlayer would contribute to improved Li-electrolyte interfacial contact. Symmetric cells were developed for validation. They were fabricated by pressing two pieces of 30 um thick lithium metal on opposite sides of an electrolyte sheet with and without Ag-C coating, as shown in **Figure 2a-b.** The cell was then subjected to a 5 MPa pressure.

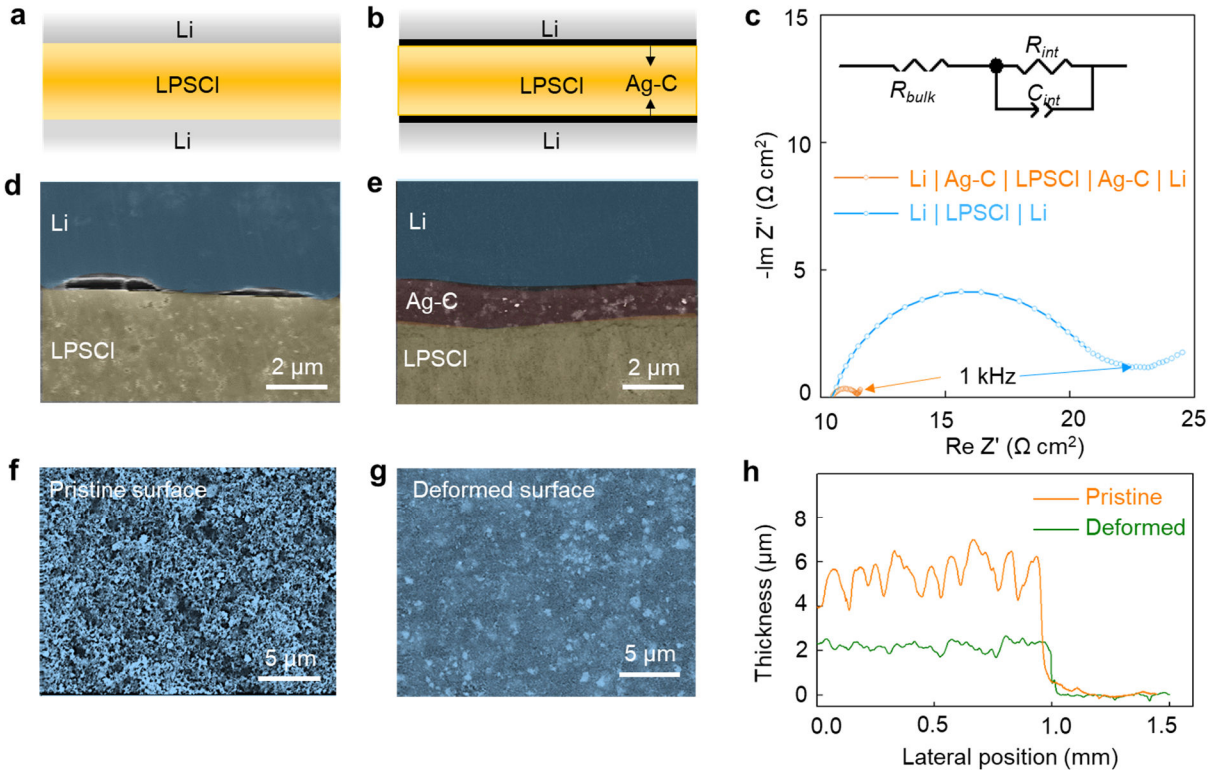


**Figure 2. The Ag-C layer improves the physical contact between Li and LPSCl for pristine cells assembled under a stacking pressure of 5 MPa**. (a, b) The cell structures are shown without and with an Ag-C layer, respectively. (c) Impedance spectra reveal an 11-fold reduction in contact resistance with the inclusion of an Ag-C layer. (d) The presence of contact loss without the Ag-C layer is visualized in a cross-sectional SEM image. (e) With an Ag-C interlayer, intimate contact between the layers is revealed without observing contact loss. (f, g) Top-view SEM images of the

Ag-C interlayer before and after calendaring under 5 MPa. (h) The surface profiles of the Ag-C interlayer before and after calendaring.

The interfacial resistance difference of symmetric cells was compared using electrochemical impedance spectra (**Figure 2c**). In the presence of an Ag-C interlayer, $R_{int}$ shinks 11-fold, from 6.59 Ω $cm^2$ to 0.58 Ω $cm^2$ (**Table S1**). We prepared two symmetric cells with exposed cross-sectional interfaces to understand the origin of the impedance reduction. An argon-ion beam cross-section polisher (JEOL IB-19520CCP) was utilized for the exposed interface specimen preparation. The polisher has a much larger cross-sectional polishing area than a standard focused ion beam machining prepared interface. We used an accelerating voltage of 4 kV under cryogenic conditions to minimize heat damage on lithium metal. In addition, to avoid the curtain effect, the sample stage was positioned perpendicular to the ion beam and swung at 30° during milling.

**Figure 2d-e** shows the cross-sectional SEM images of symmetric Li | LPSCl | Li cells with and without Ag-C interlayers. **Figure 2d** visualizes the gaps at the Li-LPSCl interface, the size of which is about 3 μm in width and the range of about 0.1~0.3 μm in height. A similar observation was reported by Sun *et al*.[21] In contrast, with an Ag-C interlayer, we observe an intimate contact among Li | Ag-C | LPSCl (**Figure 2e**). A profilometer (Bruker DektakXT) was used to characterize the interlayer thickness before and after 5 MPa pressure. **Figure 2f-h** shows the top view and thickness profiles of pristine and deformed samples, which exhibit a 72.2% reduction in roughness and a 59.7% reduction in thickness. In other words, the Ag-C interlayer functions as a mechanical buffer between Li and LPSCl, which have very different mechanical moduli.[22,23]

**Uniform current distribution between the Li anode and solid electrolyte**

The non-uniform current distribution between Li metal and solid electrolyte interfaces leads to penetration of lithium dendrites into solid electrolytes.[7] To that end, we investigate the

effects of interlayer on lithium dendrite challenges. The Ag-C interlayer is expected to stabilize the interface during cycling by homogenizing the current density. We fabricated a cell with asymmetric interfaces Li | Ag-C | LPSCl | Li (**Figure 3a)** and galvanostatically cycled it until it failed. This allows us to compare its effectiveness in preventing Li metal dendrite formation as well as identify the location of cell failure and the effect of the interlayer. **Figure 3b** shows the voltage profile of the cell while cycling at a current density of 0.16 mA $cm^{-2}$. In the fifth cycle, the cell short-circuited. Post-mortem analysis (**Figure 3c**) reveals that the cycled interfaces with and without an Ag-C interlayer differ dramatically. We observed lithium dendrite penetration into the electrolyte layer on one side where there was no Ag-C interlayer. P. Bruce *et al.* also observed similar findings with micro-computed tomography (micro CT).[8] Non-uniform lithium plating generates highly local mechanical stress in the absence of an Ag-C interlayer, causing the electrolyte to crack and Li dendrite penetration.[24] On the other hand, we observed uniform lithium plating and stripping where the Ag-C interlayer was introduced (**Figure 3e**), and the interlayer remained dense without cracking. It is critical to maintain the structural integrity of the interlayer as the volume of the Li anode changes during plating and stripping.[12]

A symmetric cell, on the other hand, is not the same as a full cell. As in a symmetric cell, the cathode side of the full cell cannot compensate for the expansion and contraction of electrodes caused by lithium metal plating and stripping during cell cycling. The volume change in full lithium metal cells is unavoidable.[25] To that end, we studied the impact of the Ag-C interlayer in full cells using NMC single crystal cathodes. The cathode composite sheet was fabricated using a tape-casting process and NMC as the cathode active material (CAM). The full cell (NMC | LPSCl | Ag-C | Li) was completed by individually pressing the cathode sheet and the Ag-C | LPSCl sheet separately at 375 MPa, then co-pressing at 375 MPa to improve adhesion between the two layers.

Finally, a thin lithium metal anode will be pressed against NMC | LPSCl | Ag-C under a stacking pressure of 5 MPa. As shown in **Figure 3f**, the operation of the NMC | LPSCl | Ag-C | Li cell was stable. The full cell without the interlayer, on the other hand, fails during the first charging to 3.7 V with a capacity of only 41 mAh $g^{-1}$. An abnormal voltage profile indicates the presence of lithium dendrites. A similar observation of SEM imaging (**Figure 3g, h**) in full cells supports the role of the interlayer in suppressing lithium dendrites by resulting in a uniform current distribution.

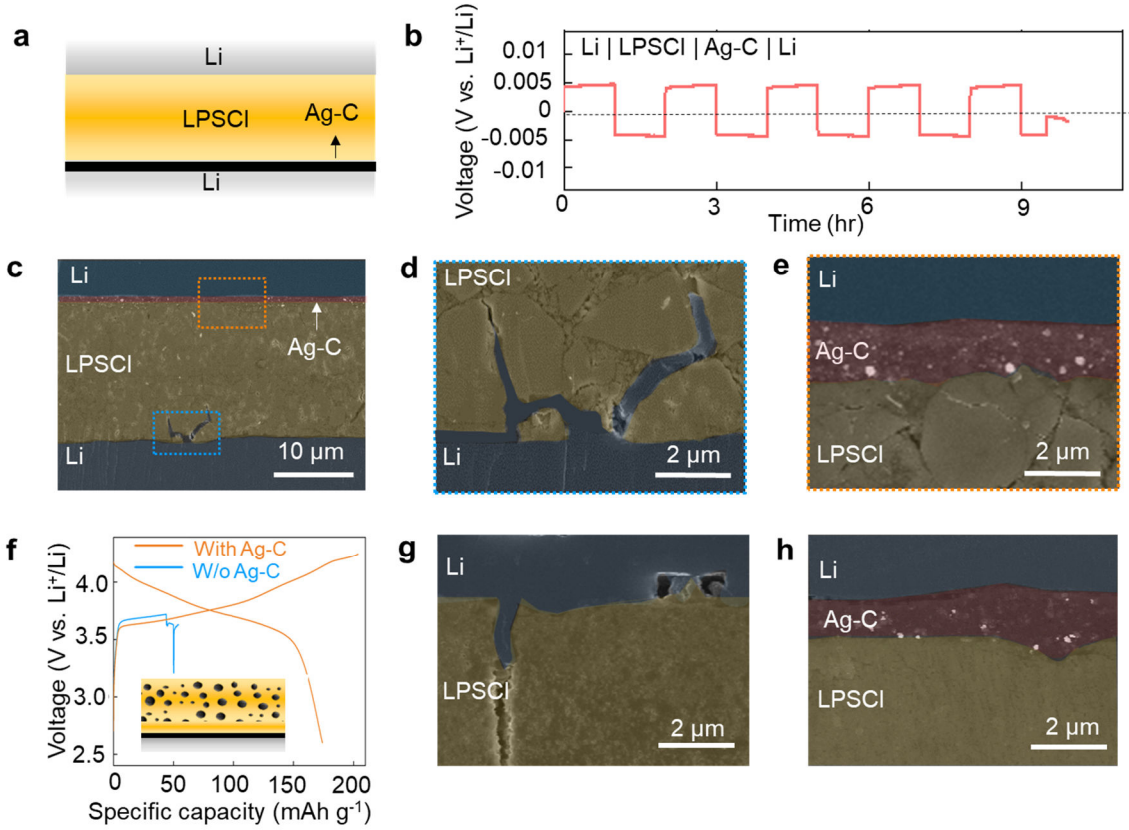


**Figure 3. Suppressing lithium dendrites with the interlayer.** (a) A cell with asymmetric interfaces. (b) Galvanostatic voltage profile at 0.16 mA $cm^{-2}$ (1-hour of plating and 1-hour of stripping) and the cell became shorted at 9.5 hour. (c-e) Post-mortem cross-sectional SEM images of the shorted cell. (f) Galvanostatic voltage profile of two full cells. The cell with the structure of NMC | LPSCl | Ag-C | Li shows a normal voltage profile during the first cycle while the cell with the structure of NMC | LPSCl | Li shows shorting during the first charge. (g-h) Post-mortem cross-sectional SEM images of the two full cells are shown in (f).

**The role of Ag in the interlayer in determining Li plating location**

The lithium plating location in a solid-state cell has been reported to be impacted by the metal particles added to the interlayer.[11] To better understand the role of Ag metal in the interlayer, we compare two types of interlayers (Ag-C *vs.* C only) in full-cell operation. The voltage profiles (**Figure S2**) show only a minor difference, but the post-mortem SEM images shows a significant difference in the location of plated lithium, as shown in **Figures 4a** and **4b**. Lithium plating occurred between the electrolyte and the interlayer in the case of the pure carbon layer. When Ag is present in the interlayer, however, lithium is plated in the desired location between the interlayer and the pristine Li anode. Despite the fact that the amorphous carbon layer provides $Li^+$ transport channels, the presence of Ag in the interlayer may facilitate Li transport.[26] Both interlayers made of Ag-C and carbon can operate at lower current densities as long as the Li flux from electrolyte is less than the Li transport capability of the interlayers. Based on our fabrication conditions (*e.g.*, carbon type and binder content), however, only Ag-C shows decent performance at higher current densities (0.16-0.8 mA $cm^{-2}$) due to its superior Li diffusivity. Conversely, inadequate Li transport in the carbon interlayer results in Li accumulation and growth at the interlayer-solid electrolyte interface. Further adjustments to the physicochemical properties of the carbon layer may enhance its high-current handling capability.

We hypothesize that the presence of Ag metal alters the interlayer diffusivity, thereby regulating the location of Li plating. The galvanostatic intermittent titration technique (GITT) was used to study the lithiation process in two asymmetric cells, carbon | LPSCl | Li and Ag-C | LPSCl | Li. **Figure S3** shows the GITT results of amorphous carbon and Ag-C interlayers at various lithiated states. The Ag-C interlayer exhibited a lower overpotential than that of the carbon interlayer, resulting in greater diffusivity of the Ag-C interlayer. **Figure 4c** summarizes the

evolution of the lithium diffusion coefficient in these two types of interlayers. At the160$^{th}$ hour of lithiation, the Ag-C interlayer has a fourfold higher diffusivity than that of the carbon-only interlayer ($1.71 \times 10^{-10}$ *vs.* $4.21 \times 10^{-11}$ cm$^2$ s$^{-1}$). When the interlayer has a high lithium diffusivity, the reduced Li atoms at the interlayer-electrolyte interface will be quickly transported toward the Li-interlayer interface and plated there because there is no nucleation barrier for Li plating on Li surface. In contrast, at low lithium diffusivity, reduced Li atoms will plate at the interlayer-electrolyte interface, despite that fact that a nucleation barrier for lithium plating exists.

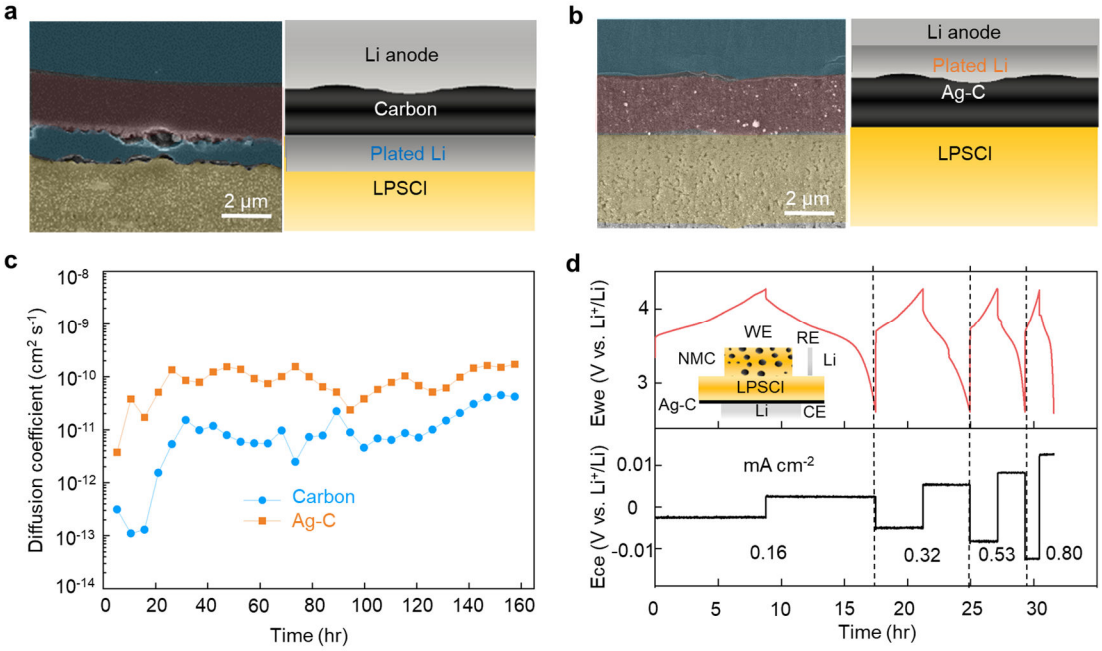


**Figure 4**. **A fully lithiated Ag-C interlayer enables lithium plating at the correct location**. (a,b) Cross-sectional SEM images and corresponding illustration of full cells after 1$^{st}$ charge. Corresponding galvanostatic voltage profiles are shown in **Figure S2**. (a) Li is plated in between LPSCl and the carbon layer while in (b) Li is plated between Ag-C and Li. (c) Comparison of the diffusion coefficients of various lithiation states of the carbon and Ag-C interlayers. Corresponding GITT voltage profiles are shown in **Figure S3**. (d) A three-electrode cell was used to separate the overpotential contribution from the cathode and anode at various rates from 0.1 C (0.16 mA cm$^{-2}$) to 0.5 C (0.8 mA cm$^{-2}$). The schematic setup of the three-electrode configuration is shown in **Figure S4**.

A three-electrode cell configuration was developed to monitor the potential of the Li anode during cell operation, revealing the interlayer's ability to regulate Li diffusivity (**Figure S4**). **Figure 4d** shows the *in situ* Li anode potential change monitored with a Li reference electrode (RE) at various cycling rates. The fact that the Li anode potential remains flat during each cycle's stripping shows no increasing polarization is observed during stripping, even at high rates.[8] The fact that the Li anode potential remains less than 10 mV at 0.8 mA $cm^{-2}$ indicates the interlayer maintains a high diffusivity. Future research will provide a quantitative description of the lithium plating regulation using an Ag-C interlayer.

**Sheet-type all-solid full cell performance**

With the Ag-C interlayer, the rate performance and cycling stability of the sheet-type full-cell were greatly improved. **Figure 5a** shows the cross-sectional image of a sheet-type full-cell setup. The overall thickness of the cell is around 100 μm. **Figure 5b** shows the voltage profiles under a stacking pressure of 5 MPa at 60℃. The cell cycled galvanostatically between 2.6 – 4.25 V. After 0.1 C, the sheet-type cell yields discharge capacities of 174.02 mAh $g^{-1}$, translating to a specific energy of 250.6 Wh $kg^{-1}$ and an energy density of 514.3 Wh $L^{-1}$, which is greater than the majority of solid electrolyte-based Li metal batteries.[27] The cell shows specific capacities of 174.0, 149.4, 130.5, 113.4 mAh $g^{-1}$, at 0.1, 0.2, 0.33, 0.5 C (1C= 200 mA $g^{-1}$). The areal capacity is 1.39 mAh $cm^{-2}$ at 0.1C. **Figures 5c and 5d** plot the capacity retention of 80.2% for 500 cycles. The average coulombic efficiency (CE) is 99.97%. Such a high CE is attributed to the Ag-C interlayer. **Figure 5e** shows the *dQ/dV* plot of the $1^{st}$, $100^{th}$, $200^{th}$, $300^{th}$, $400^{th}$, and $500^{th}$ cycles. The reduction peaks gradually shift to lower potential while the oxidation peaks shift to higher potential, indicating the increase of impedance is the main reason for the capacity decay. This is in contrast

to liquid electrolyte lithium cells where the two major mechanisms of dead lithium and electrolyte drying are absent in all solid state cells.[28]

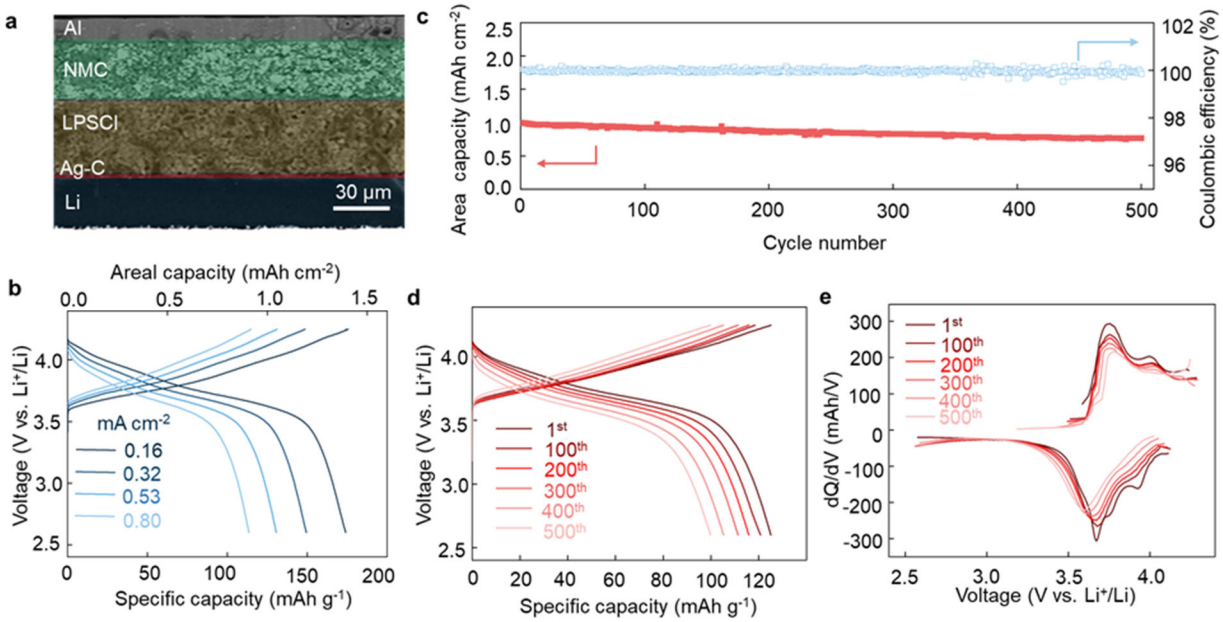


**Figure 5. Sheet-type all-solid-state lithium metal cell performance.** (a) A cross-sectional SEM image of a sheet-type all-solid-state lithium metal battery with an Al | NMC | LPSCl | Ag-C | Li device structure. (b) The rate performance of the cell at various rates from 0.1 C to 0.5 C (where 1C is equal to 1.6 mA $cm^{-2}$). (c) The galvanostatic cycle performance of the cell at C/3 rate. (d-e) The voltage profile and differential capacity (*dQ/dV*) curves for the first, 100$^{th}$, 200$^{th}$, 300$^{th}$, 400$^{th}$, and 500$^{th}$ cycles, respectively.

In conclusion, the role of the Ag-C interlayer in the solid-state cell was investigated. The Ag-C interlayer greatly improves the physical contact of the Li-electrolyte interface, which helps to homogenize the current density of the interface. Furthermore, we show how Ag metal facilitates Li transport through the interlayer. The lithiated Ag nanoparticles in the Ag-C have a high Li diffusivity, allowing lithium deposition at the desired Li-electrolyte interface. The sheet-type solid-state cell with Ag-C interlayer exhibited a superior specific energy of 250.6 Wh $kg^{-1}$ and an energy density of 514.3 Wh $L^{-1}$. The cell also demonstrated excellent cycling stability, with an average CE of over 99.97% for 500 cycles. Understanding the function of the Ag-C interlayer enables the

use of a lithium metal anode in sheet-type solid-state batteries, paving the way for the commercialization of high-energy-density solid-state batteries.

ASSOCIATED CONTENT:

**Supporting Information**

The Supporting Information is available free of charge at

http://pubs.acs.org__;!!LkSTlj0I!FJNEluXvGLiC_n7MNP7lzQfL9OK0NQ6HNc4pOjCRrtTcrTze2SP7fy7hav8X8kgMrzrXxnprWQzqce6STuDhPSbnN8FHP-jthA$

Fabrication and characterization of silver-carbon interlayer; SEM images of Li metal anode; Voltage profiles of solid-state cells; Three-electrode cell configuration (PDF).

AUTHOR INFORMATION:

**Corresponding Authors**

Zheng Fan − Department of Engineering Technology, University of Houston, Houston, TX 77204, United States; Email: fanzheng@uh.edu

Yan Yao − Department of Electrical and Computer Engineering and Texas Center for Superconductivity at the University of Houston, Houston, Texas 77204, United States; orcid.org/0000-0002-8785-5030; Email: yyao4@uh.edu

**Notes**

Zheng Fan and Yan Yao have an equity interest in Solid Design Instruments LLC. Yan Yao and Yanliang Liang have an equity interest in LiBeyond LLC.

## ACKNOWLEDGMENTS

This work was supported by the U.S. Department of Energy's Office of Energy Efficiency and Renewable Energy (EERE) under the Vehicle Technologies Program under Contact DE EE0008864.

## References

(1) Kamaya, N., Homma, K., Yamakawa, Y., Hirayama, M., Kanno, R., Yonemura, M., Kamiyama, T., Kato, Y., Hama, S., Kawamoto, K. and Mitsui, A. A lithium superionic conductor. *Nature materials* **2011**, *10* (9), 682-686.

(2) Manthiram, A., Xingwen Yu, and Shaofei Wang. Lithium battery chemistries enabled by solid-state electrolytes. *Nature Reviews Materials* **2017**, *2* (4), 1-16.

(3) Larcher, D., and Jean-Marie Tarascon. Towards greener and more sustainable batteries for electrical energy storage. *Nat. Chem.* **2015**, *7* (1), 19-29.

(4) Liu, J., Bao, Z., Cui, Y., Dufek, E.J., Goodenough, J.B., Khalifah, P., Li, Q., Liaw, B.Y., Liu, P., Manthiram, A. and Meng, Y.S. Pathways for practical high-energy long-cycling lithium metal batteries. *Nature Energy* **2019**, *4* (3), 180-186.

(5) Lau, J., Ryan H. DeBlock, Danielle M. Butts, David S. Ashby, Christopher S. Choi, and Bruce S. Dunn. Sulfide Solid Electrolytes for Lithium Battery Applications. *Adv. Energy Mater.* **2018**, *8* (27), 24.

(6) Kraft, M. A., Sean P. Culver, Mario Calderon, Felix Böcher, Thorben Krauskopf, Anatoliy Senyshyn, Christian Dietrich, Alexandra Zevalkink, Jürgen Janek, and Wolfgang G. Zeier. Influence of lattice polarizability on the ionic conductivity in the lithium superionic argyrodites $Li_6PS_5X$ (X= Cl, Br, I). *Journal of the American Chemical Society* **2017**, *139* (31), 10909-10918.

(7) Ziyang Ning, D. S. J., Guanchen Li, Robin De Meyere, Shengda D. Pu, Yang Chen, Jitti Kasemchainan, Johannes Ihli, Chen Gong, Boyang Liu, Dominic L. R. Melvin, Anne Bonnin, Oxana Magdysyuk, Paul Adamson, Gareth O. Hartley, Charles W. Monroe, T. James Marrow & Peter G. Bruce. Visualizing plating-induced cracking in lithium-anode solid-electrolyte cells. *Nature Materials* **2021**, *20* (8), 1121-1129.

(8) Kasemchainan, J., Stefanie Zekoll, Dominic Spencer Jolly, Ziyang Ning, Gareth O. Hartley, James Marrow, and Peter G. Bruce. Critical stripping current leads to dendrite formation on plating in lithium anode solid electrolyte cells. *Nature Materials* **2019**, *18* (10), 1105-1110.

(9) Lee, Y. G., Fujiki, S., Jung, C., Suzuki, N., Yashiro, N., Omoda, R., Ko, D.S., Shiratsuchi, T., Sugimoto, T., Ryu, S. and Ku, J.H. High-energy long-cycling all-solid-state lithium metal batteries enabled by silver–carbon composite anodes. *Nature Energy* **2020**, *5* (4), 299-308.

(10) Wang, Z.; Li, X.; Chen, Y.; Pei, K.; Mai, Y.-W.; Zhang, S.; Li, J. Creep-Enabled 3D Solid-State Lithium-Metal Battery. *Chem* **2020**, *6* (11), 2878-2892.

(11) Suzuki, N.; Yashiro, N.; Fujiki, S.; Omoda, R.; Shiratsuchi, T.; Watanabe, T.; Aihara, Y. Highly Cyclable All‐Solid‐State Battery with Deposition‐Type Lithium Metal Anode Based on Thin Carbon Black Layer. *Advanced Energy and Sustainability Research* **2021**, *2* (11), 2100066.

(12) Oh, J., Choi, S.H., Chang, B., Lee, J., Lee, T., Lee, N., Kim, H., Kim, Y., Im, G., Lee, S. and Choi, J.W. Elastic Binder for High-Performance Sulfide-Based All-Solid-State Batteries. *ACS Energy Letters* **2022**, *7* (4), 1374-1382.

(13) Kim, S. Y.; Li, J. Porous Mixed Ionic Electronic Conductor Interlayers for Solid-State Batteries. *Energy Material Advances* **2021**, *2021*, 1-15.

(14) Emley, B.; Liang, Y.; Chen, R.; Wu, C.; Pan, M.; Fan, Z.; Yao, Y. On the quality of tape-cast thin films of sulfide electrolytes for solid-state batteries. *Materials Today Physics* **2021**, *18*, 100397.

(15) Wang, M. J.; Kazyak, E.; Dasgupta, N. P.; Sakamoto, J. Transitioning solid-state batteries from lab to market: Linking electro-chemo-mechanics with practical considerations. *Joule* **2021**, *5* (6), 1371-1390.

(16) Tan, D. H.; Meng, Y. S.; Jang, J. Scaling up high-energy-density sulfidic solid-state batteries: A lab-to-pilot perspective. *Joule* **2022**, *6* (8), 1755-1769.

(17) Pham, V. H.; Cuong, T. V.; Hur, S. H.; Shin, E. W.; Kim, J. S.; Chung, J. S.; Kim, E. J. Fast and simple fabrication of a large transparent chemically-converted graphene film by spray-coating. *Carbon* **2010**, *48* (7), 1945-1951.

(18) Azarova, N. A.; Owen, J. W.; McLellan, C. A.; Grimminger, M. A.; Chapman, E. K.; Anthony, J. E.; Jurchescu, O. D. Fabrication of organic thin-film transistors by spray-deposition for low-cost, large-area electronics. *Organic Electronics* **2010**, *11* (12), 1960-1965.

(19) Doux, J. M.; Nguyen, H.; Tan, D. H.; Banerjee, A.; Wang, X.; Wu, E. A.; Jo, C.; Yang, H.; Meng, Y. S. Stack pressure considerations for room‐temperature all‐solid‐state lithium metal batteries. **2020**, *10* (1), 1903253.

(20) Hänsel, C.; Kundu, D. The Stack Pressure Dilemma in Sulfide Electrolyte Based Li Metal Solid‐State Batteries: A Case Study with $Li_6PS_5Cl$ Solid Electrolyte. *Advanced Materials Interfaces* **2021**, *8* (10), 2100206.

(21) Sun, M.; Liu, T.; Yuan, Y.; Ling, M.; Xu, N.; Liu, Y.; Yan, L.; Li, H.; Liu, C.; Lu, Y. Visualizing lithium dendrite formation within solid-state electrolytes. *ACS Energy Letters* **2021**, *6* (2), 451-458.

(22) Singh, D. K.; Henss, A.; Mogwitz, B.; Gautam, A.; Horn, J.; Krauskopf, T.; Burkhardt, S.; Sann, J.; Richter, F. H.; Janek, J. $Li_6PS_5Cl$ microstructure and influence on dendrite growth in solid-state batteries with lithium metal anode. *Cell Reports Physical Science* **2022**, *3* (9), 101043.

(23) Masias, A.; Felten, N.; Garcia-Mendez, R.; Wolfenstine, J.; Sakamoto, J. Elastic, plastic, and creep mechanical properties of lithium metal. *Journal of materials science* **2019**, *54* (3), 2585-2600.

(24) LePage, W. S.; Chen, Y.; Kazyak, E.; Chen, K.-H.; Sanchez, A. J.; Poli, A.; Arruda, E. M.; Thouless, M.; Dasgupta, N. P. Lithium mechanics: roles of strain rate and temperature and implications for lithium metal batteries. *Journal of The Electrochemical Society* **2019**, *166* (2), A89.

(25) Ham SY, Y. H., Nunez-cuacuas O, Tan DH, Chen YT, Deysher G, Cronk A, Ridley P, Doux JM, Wu EA, Jang J, Meng, Y. S. Assessing the Critical Current Density of All-Solid-State Li Metal Symmetric and Full Cells. *Energy Storage Materials* **2023**, *55*, 455-462.

(26) Feng, W.; Dong, X.; Zhang, X.; Lai, Z.; Li, P.; Wang, C.; Wang, Y.; Xia, Y. Li/Garnet Interface Stabilization by Thermal-Decomposition Vapor Deposition of an Amorphous Carbon Layer. *Angew Chem Int Ed Engl* **2020**, *59* (13), 5346-5349.

(27) Simon Randau, D. A. W., Olaf Kötz, Raimund Koerver, Philipp Braun, André Weber, Ellen Ivers-Tiffée, Torben Adermann, Jörn Kulisch, Wolfgang G. Zeier, Felix H. Richter & Jürgen Janek. Benchmarking the performance of all-solid-state lithium batteries. *Nature Energy* **2020**, *5* (3), 259-270.

(28) Gao, N.; Abboud, A. W.; Mattei, G. S.; Li, Z.; Corrao, A. A.; Fang, C.; Liaw, B.; Meng, Y. S.; Khalifah, P. G.; Dufek, E. J. Fast diagnosis of failure mechanisms and lifetime prediction of Li metal batteries. *Small Methods* **2021**, *5* (2), 2000807.

**TOC**

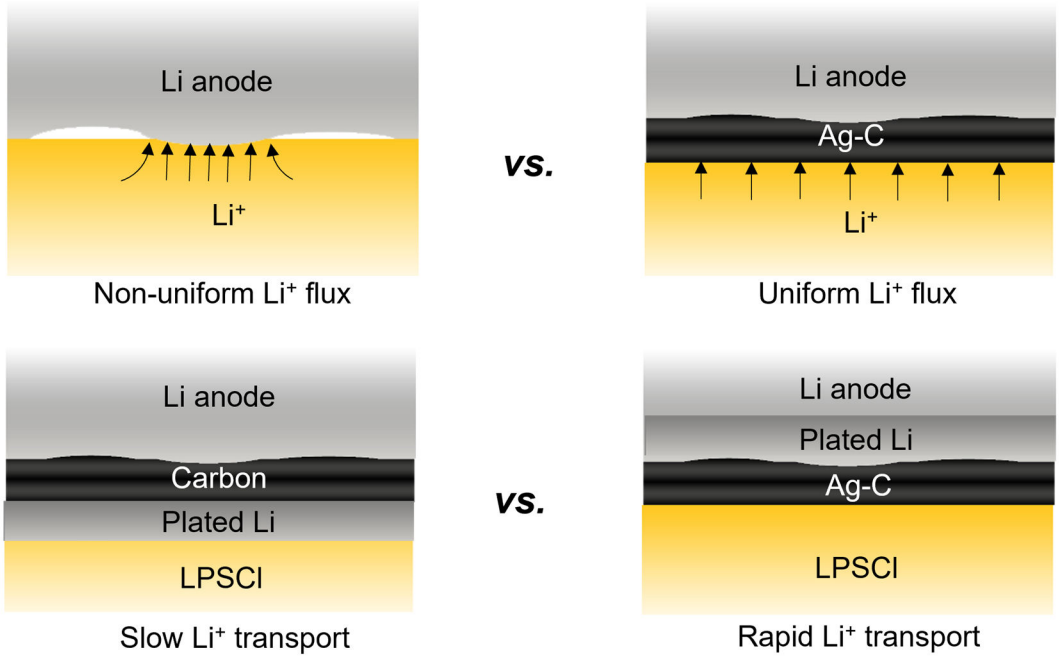
Li anode
Li⁺
Non-uniform Li⁺ flux
vs.
Li anode
Ag-C
Li⁺
Uniform Li⁺ flux
Li anode
Carbon
Plated Li
LPSCl
Slow Li⁺ transport
vs.
Li anode
Plated Li
Ag-C
LPSCl
Rapid Li⁺ transport